Influence of the dimensions of spheroniser plate protuberances on the production of pellets by extrusion-spheronisation

M. Zhang[a*], X. K. Li[b], D. I. Wilson[c], T. T. Yao[a] and Y. Y. Zhang[a]

[a]*School of Pharmacy, Xi'an Jiaotong University, No. 76, Yanta West Road, Xi'an, Shaanxi 710061, PR China*
[b]*School of Chemical Engineering, Xi'an University, No. 1,Ke Ji Road, Xi'an, Shaanxi 710065, PR China*
[c]*Department of Chemical Engineering and Biotechnology, University of Cambridge, West Cambridge Site, Philippa Fawcett Drive, Cambridge, CB3 0AS,UK*

Abstract

The influence of the dimensions of square-patterned pyramidal protuberances on a spheronisation plate on pellet yield, size and shape distributions, surface tensile strength and surface morphology was investigated using a 45 wt% microcrystalline cellulose/water paste. Tests were conducted using four extrudate diameters (1.0, 1.5, 2.0 and 2.5 mm) generated by screen extrusion and seven plate geometries, including a flat plate as a control. Geometrical analyses of the protuberance shapes provide some insight into the observed differences. Sharper protuberances reduced yield (promoting breakage and attrition) but tended to give narrower size distributions and less even pellet surfaces. The pellet yield for 1 mm extrudates was also subject to losses caused by fragments passing through the 1.0 mm gap between the plate and the spheroniser wall. Pellet tensile strengths were noticeably greater for 1.0 mm diameter extrudates, which is attributed to the greater extensional strain imparted on the paste during the extrusion step. For some geometries there is an optimal ratio of extrudate to protuberance dimensions.

Keywords: spheronisation; screen extrusion; friction plate pattern; shape; size; tensile strength.

[*] Corresponding author

E-mail address: mz282@cantab.net/m.zhang904@xjtu.edu.cn (M. Zhang).

1. Introduction

Extrusion-spheronisation (E-S) is a favoured pelletisation process in the pharmaceutical, food and catalyst industries since it can generate dense pellets with an almost spherical shape, a narrow size distribution and smooth surfaces [1]. These properties enable the pellets to deliver controlled dosage and also allow further processing steps (such as coating and tableting) to be carried out relatively easily. E-S features four steps, namely combination, extrusion, spheronisation, and drying and finishing [2]. In the combination step, dry powders (*e.g.* excipients, active pharmaceutical ingredients) are mixed with a liquid binder to produce a wet mass, which is also known as a paste. The paste is then loaded into an extruder where it is compacted and forced to flow through the holes in a die or screen to generate long cylindrical extrudates. In the spheroniser, essentially a rotating friction plate, the extrudates break up and are rounded into pellets which are then dried and coated as required. For pharmaceutical tableting and capsuling, the pellets are required to be within the size range 0.5 – 1.5 mm [3].

The design and optimisation of an E-S process requires a good understanding of the relationship between the raw material properties, paste rheology, processing conditions and pellet quality. Optimisation is currently based on empirical approaches, the results of which may be interpreted by data fitting methods based on generic models such as response surface methodologies (*e.g.* [4]): this usually requires large amounts of material and experimental time. Another approach is to establish the governing physical mechanisms from experiments, and to construct physical-mathematical models [5] which can be then used to interpret the experimental data and provide guidance for optimisation, such as in the selection of groups of variables to be manipulated. The mechanisms governing spheronisation are not completely understood, and this paper describes an investigation of the influence of the spheroniser plate geometry, which will help to elucidate the mechanisms involved.

Screen extrusion is commonly used in industry where high throughput is a priority. Zhang *et al.* [6] recently demonstrated a novel laboratory device for studying screen extrusion of pharmaceutical pastes and its use in developing new formulations for screen E-S. Most of the investigations of paste extrusion, however, have focused on ram [7-11] and screw varieties [12-14].

Quantitative physical methods, such as the Benbow-Bridgwater approach, are available to characterise the paste rheology during such operations [15]. By comparison, the understanding of material-machine interactions in spheronisation is poor. Various groups have used high speed video techniques to track the motion of extrudates and pellets [16-17]: in brief, the extrudates are initially accelerated towards the outer rim of the spheroniser plate and are subsequently dragged around circumferentially in a rope. They experience collisions with the wall, with the plate, and with each other in a complex flow pattern. Rough and co-workers [18-19] showed that ram extruded extrudates undergoing spheronisation passed from a breakage to a rounding stage and presented a dimensional analysis of the process [20].

Influence of the spheronisation plate

There are three mechanical parameters involved in spheronisation: the radius of the spheronisation plate, R; the rotation speed, ω; and the geometry of any protuberances on the plate. The rim speed, given by $R\omega$, is used in design and scale-up. Since the pellets spend most of the time in the rope, $R\omega$ sets the characteristic velocity in collisions. Video analyses (*e.g.* [20]) confirmed that pellet velocities were of order $R\omega$, and usually significantly below this value.

By comparison, there is little in the published literature on screen extrudate-spheroniser interactions and their effect on pellet quality. The influence of plate groove geometry on pellet size, shape and surface morphology has not been studied in depth. The groove shape and dimensions, also known as the hatching pattern, refers to the arrangement of groove lines on a plate surface. Table 1 is a summary of systematic studies of protuberance size and shape performed to date. As part of this study we introduce the geometrical parameters d^*, D^*, θ and α (defined in the next section) and these are reported in Table 1 to allow comparison of the current work with previous investigations.

Michie *et al*. [21] compared pellets obtained from three plates with different hatching patterns, namely cross-hatched, radial-hatched and striated edge patterns (Figure 1 in [21] shows images of the plates). They generated 1.0 and 1.5 mm diameter extrudates using an industrial scale screen extruder. Differences in the groove line arrangements and the extrudate diameter resulted in noticeable differences in spheronisation yield, median pellet size, pellet mechanical strength and porosity. They found that a cross-hatched pattern plate gave a high pellet tensile strength and porosity, accompanied by a lower yield and smaller percentage of pellets within the desired range compared to the other two plates. They did not investigate the influence of protuberance size and shape for the same hatching pattern. This is the subject of the current study.

On radial and striated pattern plates the protuberance size and shape change with radial location. These features on a cross-hatched pattern are independent of plate radius, which benefits scale-up and has promoted industrial interest in cross-hatched patterns. Given that the solids only interact with the outer ring of the plate for the majority of the spheronisation

process, the size and shape of the protuberances in this region are expected to determine the dynamics of the bed.

Schmidt and Kleinebudde [22] investigated two cross-hatched plates, both with pyramidal protuberances. The protuberances differed in their dimensions (see Table 1). Their work suggested that tall protuberances with a larger base (Table 1: H = 1.5 mm, $W \times W$ = 9.0 mm^2) led to a rough surface, generating pellets of a large median diameter and a broad size distribution.

Liew *et al*. [23] investigated spheronisation of screen-extruded material on two cross-hatched plates, one with pyramidal protuberances and the other teardrop-studded ones (see Figure 2 in [23]). The former generated larger and more spherical pellets at a rim speed of 10 m s^{-1}, and they attributed the differences in pellet size and shape to the amount of frictional force experienced by the extrudates. They asserted that, compared to the pyramidal protuberances at a given rim speed, the teardrop studs imparted fewer and weaker frictional interactions due to their rounded shape and smaller number per unit area. Since the protuberance size and shape differed, it was not possible to separate the effect of these parameters.

Zhang *et al*. [24] investigated spheronisation of 1.0 and 2.0 mm screen extrudates using four cross-hatched plates which differed either in protuberance size or shape (see Figure 2 in [24]). Both size and shape had significant effects on pellet yield, size, shape and surface morphology. Compared with saw-toothed protuberances, pyramidal ones gave pellets with a narrower size and shape distribution, and smoother surfaces. These results indicated the need to systematically study how the ratio of the extrudate diameter to protuberance size influences spheronisation. One complication is that the strain experienced by the paste during screen

extrusion, and thereby its strength (*i.e.* its rheology), is related to the diameter and spacing of the screen holes, while the diameter of the extrudate determines how it interacts with the protuberances (*via* geometry).

This study extends earlier work [24] on the influence of extrudate diameter, *D*, and protuberance dimensions. Testing employed a 45 wt% MCC/water paste which has been employed previously as a model formulation to investigate E-S mechanisms [6, 19, 24-26]. Extrudates were generated using a basket screen extruder with screen hole diameters ranging from 1.0 to 2.5 mm, allowing *D* to be varied. Preliminary tests showed that these extrudates could produce pellets in the size range, after drying, of 0.5 – 1.5 mm.

Pellets are compared in terms of spheronisation yield, water content, pellet size and shape distribution, surface tensile strength and surface morphology. The results provide insight into the spheronisation mechanism and guidance for design or selection of E-S equipment for generation of pharmaceutical pellets.

2. Spheroniser plate geometries

Six spheroniser plates of diameter 120 mm were manufactured from 304 stainless steel with pyramidal protuberances in a cross-hatched surface pattern. Schematics of the pattern, introducing the geometry and characteristic dimensions, are given in Figure 1. The dimensions for each plate (labelled A to F) are given in Table 2. A flat, smooth plate (polished, surface roughness less than 1 μm, labelled X) was employed as a control. Table 2 reports four metrics which were used to characterise the plate geometries.

Pyramid sharpness, θ

Angle θ quantifies the sharpness of the top edge of the pyramid, which is expected to affect breakage when extrudates strike the plate surface, as well as erosion of material from pellets during rounding and indentation.

$$\theta = \tan^{-1}\left(\frac{S-W}{2H}\right) \quad [1]$$

Area fraction, α

This quantifies the amount of flat surface, provided by the pyramid tops, in contact with the solids. A large value of α is expected to reduce the influence of furrow geometry.

$$\alpha = \frac{W^2}{S^2} \quad [2]$$

Critical extrudate diameter, D^*

Extrudates with a small diameter are expected to be able to collect or rest in the furrows between protuberances, affecting the interaction of the bed with the plate. For each protuberance shape a critical extrudate size can be calculated, as shown in Figure 1(*b*).

$$D^* = \left[\frac{1}{4H^2} + \frac{1}{\left(S\text{-}W\right)^2}\right]^{-1/2} \quad [3]$$

Critical pellet diameter, d^*

Following similar arguments to D^*, the 'seat' between four adjacent protuberances can give rise to a critical pellet size (assuming spherical pellets), as shown for a spherical pellet in Figure 1(*c*), and is calculated thus:

$$d^* = \left[\frac{1}{4H^2} + \frac{1}{2\left(S\text{-}W\right)^2} \right]^{-1/2} \qquad [4]$$

A second characteristic pellet diameter arises from breakage considerations. Wilson and Rough [2] reported that pellet sizes were often distributed around a characteristic size, with the latter being the diameter of a sphere whose volume was equal to the volume of a cylinder (*i.e.* extrudate) with length equal to its diameter. This characteristic size is labelled d_D:

$$d_D = D\sqrt[3]{3/2} \cong 1.15D \qquad [5]$$

3. Material and methods

3.1 Material

Microcrystalline cellulose (MCC, Avicel PH101) powder was obtained from FMC biopolymer™ (FMC Corporation, Philadelphia, USA). The moisture content of the as-received MCC powder was approximately 2 wt%. Particle sizing analysis was performed using a Beckman Coulter™ LS13320 laser diffraction particle size analyser (Beckman Coulter, Inc., USA), giving a particle size range of 1.7 – 340 μm with D[3,2] ≈ 46 μm. Deionised water was used to prepare suspensions for particle sizing analysis and to prepare pastes.

3.2 Experimental

3.2.1 Paste preparation

The 45 wt% MCC/water paste was prepared following the procedure reported by Zhang *et al*. [24]. MCC powder and deionised water were weighed out using an electronic balance (± 0.01 g, PL1502E, Mettler-Toledo Ltd., Shanghai, China). The powder was loaded into the bowl of a planetary mixer fitted with a K-shaped beater (Chef Classic KM353, Kenwood Ltd., Shanghai, China), and deionised water then poured slowly into the bowl over a period of one minute while the beater stirred at its minimum speed. The mixture was stirred for another 10 minutes, during which mixing was performed at dial setting speeds of 1, 2, 3 and 4 for 2, 3, 3 and 2 minutes, respectively. The process was interrupted at the end of each period and paste built up on the walls returned to the bowl by a wooden spatula. After mixing, the paste was placed in a plastic sample bag, sealed and held at room temperature for at least one hour before extrusion, which allowed the water to equilibrate through the paste. Paste was discarded after 7 hours.

3.2.2 Extrusion-spheronisation

Extrudates were generated using a lab-scale basket screen extruder (ZLB-80, Cheng Hang Xin Rong Hua Manufacturer, Zhang Jia Gang, China) manufactured from 304 stainless steel with a screen inner diameter of 84 mm. Four screens with hole sizes of 1.0, 1.5, 2.0 and 2.5 mm diameter were available. The holes were manufactured by punching and the dimensions of the screens are summarised in Table 3. The gap between the blade and the inner side of the screen was 1.0 mm. Extrusions were performed at a blade rotational speed of 52 rpm, generating a shear rate in the nip of 226 s^{-1}.

Spheronisation was performed on a 120 mm diameter bench-scale unit (R-120, Chong Qing Li Pu Pharmaceutical Equipment Manufacturer, Co. Ltd., Chong Qing, China). The spheroniser plates (see Table 2) and the spheroniser chamber were constructed from 304 stainless steel. Spheronisation runs used about 30 g of fresh extrudates and a plate rotational speed of 1600 rpm (corresponding to a rim speed of 10 m s^{-1}) for 6 min. Each experiment was repeated at least twice to confirm its reproducibility.

3.2.3 Drying

The water content of paste, extrudate and pellet samples was determined from the mass loss on drying in a hot air oven at 60 ^{o}C. The percentage yield of pellets on a dry basis, *Y*, was calculated from

$$Y(\%) = \frac{m_{\mathrm{p}} \times (100 - w_{\mathrm{p}})}{m_{\mathrm{ex}} \times (100 - w_{\mathrm{ex}})} \qquad [6]$$

where m_{p} is the mass of fresh pellets obtained after spheronisation, w_{p} their water content (in wt%), m_{ex} the mass of fresh extrudates loaded into the spheroniser and w_{ex} their water content. The percentage lost, *i.e*. 100-*Y*, gives an indication of the total amount of solid lost as fines.

Each test was repeated at least three times and the average, $\bar{Y}$, is reported.

3.2.4 Pellet characterisation

Dry pellets were firstly sieved using a 2.0 mm mesh to remove large pellets, followed by a 0.335 mm mesh to separate out smaller ones, labelled as fines. About 150 pellets were then selected using a riffler for further analysis. Pellet size and shape were determined using an image analysis system (BT-1600, Bettersize Instrument Ltd, Dandong, China), fitted with a 0.7× magnification lens. The circle equivalent diameter, d_{CE}, is reported as the pellet size parameter, and the aspect ratio is used as the shape parameter (see [11,18]). One-way analysis of variance analysis (ANOVA) and principal component analysis (PCA) were carried out using the SPSS Statistics 17.0 package. For ANOVA analysis, the difference is considered significant if the F statistic is noticeably larger than 1.0 and the statistical significance (P) is not larger than 0.05.

The coefficient of quartile variation (CQV) was used to quantify the spread of each pellet size and shape data set, calculated using [27]

$$\mathrm{CQV} = \frac{Q_3 - Q_1}{Q_3 + Q_1} \qquad [7]$$

where Q_1 and Q_3 are the 25% and the 75% percentiles, respectively.

For each batch, the extent of shrinkage on drying was determined by measuring d_{CE} of ten pellets before and after drying using image analysis. The pellet samples were selected randomly. Most tests were run twice and the data showed good reproducibility. The pellet dimensions were found to decrease by about 26%, irrespective of the initial extrudate diameter and protuberance size. The diameter of a dried pellet is therefore expected to be

$$d_{\mathrm{dry}} = d_{\mathrm{D}} \times (1 - 0.26),$$

Combining this result with Eq. 5 yields

$$d_{\mathrm{dry}} = 1.15D \times 0.74 \qquad [8]$$

The force required to crush the pellets was measured on a pellet crushing force analyser (± 0.1 N, Hai Nan Haibo Lab equipments Co., Ltd.; model: HB-KQD; max. load: 500 N). Individual pellets were placed at on the midpoint of the lower of two parallel plates and the upper plate moved down slowly. The maximum force at failure was recorded as the crushing force of the pellet, F_{c}. About 25 pellets were tested per batch and the pellet surface tensile strength, σ_{t}, was calculated from the average of F_{c} via [28].

$$\sigma_{\mathrm{t}} = 0.4 \frac{F_{\mathrm{c}}}{\pi \left(\frac{\bar{d}_{\mathrm{CE}}}{2} \right)^2} \qquad [9]$$

where $\bar{d}_{\mathrm{CE}}$ is the median circle equivalent diameter of the pellets (see above).

Scanning electron microscopy (SEM, TM-1000, Hitachi Ltd, Japan) was used to investigate the surface morphology of randomly selected dry pellets. The pellets were sputter coated with a thin layer of platinum before imaging at 15 kV under vacuum at 60× magnification.

4. Results and Discussion

4.1Spheronisation yield

Yield is calculated using Eq. 6, and expresses the mass of dry pellets recovered after spheronisation. Material is lost via the formation of fines, which are not recovered from the plate, and from fines and fragments which are lost through the 1 mm gap between the plate and the spheroniser wall. The results are presented in the form $\bar{Y}$ against extrudate diameter in Figure 2, with plates grouped together based on similarity in trend. The results for the flat plate, X, are given in each plot as the control. For a given extrudate diameter(r, plates E and D give the lowest and the highest yields, respectively, and the difference between the seven plates is significant (D = 1.0 mm: F = 12.014, P = 0.001; D = 1.5 mm: F = 10.526, P = 0.001; D = 2.0 mm: P(Welch) = 0.033, P(Brown-Forsythe) = 0.017; D = 2.5 mm: P(Welch) = 0, P(Brown-Forsythe) = 0.005).

The yield obtained with the flat plate increases gently with extrudate diameter, which can be attributed to two mechanisms which will also be active with other plates. The first is termed *gap loss*, arising directly from breakage. Following collisions, the extrudates break into segments (shorter cylindrical sections) of varying length, l. The l/D ratio determines the segment's behaviour during the rounding stage [18, 26]. Many of the D = 1.0 mm extrudates gave long segments (*i.e.* $l/D \geq 1.5$: [26]) but a fraction gave short segments ($l/D < 1.5$) which were then prone to be lost through the 1 mm plate-wall gap. With the exception of plate B, all plates gave lower yields for D = 1 mm. The choice of l/D = 1.5 as the division between long and short segments was proposed by Lau *et al*. [18] and Zhang *et al*. [26]. The fraction of extrudates giving long segments decreased as D increased: for the 2.5 mm extrudates, most of them broke into short segments but this would not lead to gap loss as the diameter was then larger than the gap.

For D> 1 mm the loss of about 2% is attributed to generation of fines. This is postulated to be due to the difference in the rheology of the extrudates. Bryan *et al*. [29] reported that more fines were generated in spheronisation of a model paste similar to that used here when extruded through two different devices: the stiffer extrudates gave noticeably more fines on breakage. The strain experienced by the material undergoing screen extrusion is related to the hole area fraction (see Table 3) and the extrudates with small D are then likely to be stiffer than those with large D. Quantitative evidence of extrudate stiffness has been identified as an area for future work, and may require technique development [26].

The effect of D via stiffness and breakage for D > 1 mm on the flat plate is mild. Figure 2(*a*) shows that similar trends were observed with plates C and D, with superior yield for 1.5 mm extrudates. The lower yields for 1 mm extrudates are attributed to gap loss. Plates C and D featured D^* values of 1.8 mm and 1.4 mm (see Table 2), respectively, suggesting that 1.5 mm extrudates and their segments could sit in furrows periodically, altering the interactions between the plate and bed, which reduce the velocity of collisions and thereby the attrition rate. This interaction would not be available for 2.0 and 2.5 mm extrudates, and similar results to X are obtained. Detailed motion analysis is suggested to verify this hypothesis. Plates C and D also featured more oblique protuberances, with θ values of 63° and 45°, respectively, and this is expected to result in less attrition in paste/protuberance collisions. Schmidt and Kleinebudde [22] also reported that taller protuberances (lower θ) give higher friction surfaces.

Figure 2(b) shows the effect of D^* for smaller values of θ (*i.e.* sharper protuberances) to be significant (P(Welch test) = 0.021, P(Brown-Forsythe test) = 0.008). For D> 1.5 mm, yield decreases progressively with increasing D, with greatest loss for plate E (with sharpest

protuberances, θ=14°). The decrease is noticeably milder for plate F, which differs from A, B and E in the value of D^* (at 1.8 mm compared to less than 1 mm). The D^* value of plates A, B and E is less than 1 mm so extrudates with diameter 1 mm or greater are less likely to sit in the furrows (as discussed above): the extrudates and pellets are expected to experience higher velocities on the plates, and contact with sharp protuberances is more likely to result in attrition.

Plate F has a noticeably larger value of d^* than the other three plates with sharp protuberances, with d^* = 2.3 mm compared to $\leq$ 1.3 mm for plates A, B and E. Pellets are expected to be able to occupy the seat in this plate (as with extrudates and D^*), modifying the friction interaction and collision history (*i.e.*, the number of and force involved in collisions that material experiences). Michie *et al*. [21] also reported a reduction in yield at higher D for all three striation patterns tested. They did not report the protuberance dimensions, so it is not possible to say whether their findings confirm this result for θ.

In terms of the shape metrics, the effect of d^*, D^* and θ on spheronisation yield is significant, as one-way ANOVA analysis gives P(Welch test) = 0.003 and P(Brown-Forsythe test) = 0.001, P(Welch test) = 0.004 and P(Brown-Forsythe test) = 0.001, and P(Welch test) = 0.005 and P(Brown-Forsythe test) = 0.001, respectively. There is no evident correlation between yield and area fraction, most likely because the range of α values is admittedly small.

4.2 Pellet characterisation

Dried material recovered from the spheroniser plate was initially sieved using a pair of meshes to remove undersize (<0.355 mm) and oversize (>2.0 mm) pellets. The mass percentages of excluded fractions are given in Table 4. For most cases the excluded pellets constituted less than 1% of the product. For the largest extrudate diameter, d_{dry} (when dried, Eq, 8) is 2.13 mm so some oversized pellets were expected. Noticeable amounts of oversized pellets were obtained with plates C and D, at 31% and 40%, respectively, with a milder fraction of 4.8% for plate F. These were also the plates with largest yield for D = 2.5 mm: this result is consistent with these protuberance patterns subjecting extrudates to less energetic collisions, reducing attrition and breakup, and allowing agglomeration.

Pellets in the 0.355 to 2.0 mm size range, which were considered acceptable for pharmaceutical applications, were subjected to image analysis and the size and shape distributions are summarised in Figure 3. The pellet sizes are presented in dimensionless form, d_{CE}/D. It is noticeable that few pellets were obtained with $d_{CE}/D > 1$, for all extrudate sizes.

Inspection of the aspect ratios indicates that all the pellets obtained from plates with protuberances were of acceptable shape. There is little variation in aspect ratio and the median values lay in the range of 0.92-0.95, which is larger than the threshold of 0.80 suggested by Chopra *et al*. [30]. Plate X gave a median aspect ratio of 0.92 for D = 1 mm (detailed in Supplementary Figure S1), indicating that rounding on the flat plate was not as efficient as on the patterned plates. Similar results were obtained by Liew *et al*. [23] for 1 mm extrudates on a larger spheroniser plate with cross-hatched pyramidal protuberances (see Table 1). They reported their results in terms of the elongation ratio, which is the inverse of the aspect ratio employed here: their value of 1.085 is equivalent to an aspect ratio of 0.92.

The pellet size distributions were classified as uni, bi- or tri-modal, with or without a shoulder and the results are listed in Table 5. There is more variation for D = 1 and 1.5 mm extrudates: for larger extrudates the distributions were mostly unimodal (with the exception of the flat plate, X).

From Equation [8], the expected average pellet size after drying is $d_{dry} = 0.85D$. Figure 4 shows that the median d_{CE}/D value for nearly all the plates for $D \leq 2$ mm was approximately 0.74. This corresponds to an undried median pellet diameter essentially equal to that of the extrudate. The exception was plate E, which gave $d_{CE}/D = 0.64$ at $D = 2$ mm.

There is a noticeable difference between plates C and D and the other plates for the largest extrudates: the median d_{CE}/D value for C and D remained near 0.74 whereas it decreased for all the others, including the flat plate, towards 0.60. This is consistent with plates C and D giving significant amounts of large pellets with D = 2.5 mm (Table 4). Plates C and D also gave unimodal distributions at high D. One-way ANOVA shows that the effect of D on median d_{CE}/D of plates X, A, B, E and F is significant ($F = 36.858$, $P = 0$).

The effect of D on pellet size range (as quantified by the difference between the 75% and 25% percentile values) is also significant, as ANOVA analysis (excluding data from $D = 2.5$ mm extrudates using plates C and D) gives $F = 4.252$ and $P = 0.016$. The pellet size range (indicated by range bars in Figure 4) from the 1.0 and 1.5 mm extrudates is generally larger than that of pellets from 2.0 and 2.5 mm extrudates when a given plate is used for spheronisation.

The variation in the number of modes and median values of the size distributions arises from the breakage process, as this determines the amount of material in the fragments that undergo subsequent rounding. The shift to lower d_{CE}/D values does not appear to be related to D^* or d^* for the plates with protuberances, and ANOVA analysis gives $F = 0.742$ and $P = 0.602$ for D^*, and $F = 0.942$ and $P = 0.461$ for d^*. Sharper protuberances E (14°: D = 2 mm) appear to promote the transition before A, B, F (27°, 28°; D = 2.5 mm) and C, D (> 40°; D> 2.5 mm) but the trend is not statistically significant, with $F = 0.793$ and $P = 0.544$. In contrast, Schmidt and Kleinebudde [22] found that high protuberances gave large pellets (see Table 1)

The reason why the transition with the flat plate is similar to A, B, and F requires further investigation. Pellets from plate X also gave broader size distributions than the other plates (ANOVA, comparing X with A – F: $F = 5.759$, $P = 0.024$). The aspect ratio range, as quantified as the difference between the 75% and 25% percentiles, of pellets from plate X is also significantly larger than that of pellets from plates A – F ($F = 10.222$, $P = 0.004$: see Supplementary Figure S1). Protuberances narrow the pellet size and shape distribution, possibly at the expense of generating fines.

These results highlight how the mechanisms governing break-up in these systems require further elucidation: the momentum of the extrudates increases with the size of extrudates by D^2 but how this determines the number and size of segments is not currently understood.

4.3 Pellet surface tensile strength

The average pellet surface tensile strength data in Figure 5 show a statistically significant effect of D on pellet tensile strength ($F = 24.525$, $P = 0$). The strengths of the pellets from D = 1.5, 2.0 and 2.5 mm extrudates are not statistically different (P(Welch test) = 0.054, P(Brown-

Forsythe test) = 0.129), while the strength of the pellets generated from D = 1.0 mm extrudates is significantly higher (see the Post Hoc Least Squares Difference (LSD) results in Table 6). There is no significant effect of protuberance dimensions on pellet tensile strength (F = 0.374, P = 0.887). The results indicate that the extrudate diameter, but neither the protuberance dimensions nor the pellet size distributions, has a significant effect on the pellet tensile strength. Given that the pellet sizes were similar, the difference in strength is expected to arise from the material rheology. As mentioned above, the 1 mm extrudates were expected to be stiffer as they experienced the largest strain during preparation. The similarity of strengths for D = 1.5 and 2.0 mm is consistent with the similar strain histories during extrusion (Table 3).

The values of crushing strength can be compared with earlier studies. Liew *et al*. [23] reported crushing force and pellet size in terms of the mass median diameter, which yields an estimated crushing strength of 0.9 – 1.0 MPa, albeit for a different formulation and different extrusion device. Michie *et al*. [21] reported pellet tensile strengths in the range of 3 – 7 MPa for different studies, including those in Table 1, for a different formulation (10 g diclofenac sodium, 40 g lactose monohydrate, 150 g MCC and 135 g distilled water) using different spheronisation plates.

4.4 Pellet surface morphology

The SEM images of pellets in Figure 6 allow surface defects and smoothness to be gauged. This information is not available from the pellet shape and size techniques. Pellets generated using plates X and D have few surface defects (holes, cracks and dents). These are the plates with more oblique angles, with θ = 90^o and 63^o for X and D, respectively. There is no consistent trend for plates with $\theta \leq$ 45^o: plates A, B and E give relatively even surfaces for $D \geq$ 2 mm, whereas pellets generated using C and F from similar extrudates were dimpled.

Visual inspection suggests that pellets with $D/d^* > 1.5$ tended to be smoother: in this case, the pellet bed would be more likely to roll over the plate, promoting collisions from many contacts and thus rounding. More energetic collisions are expected to result in dents and cracks.

Zhang *et al*. (2016a&b) also reported differences in the surface morphology of pellets generated from 1.0 and 2.0 mm diameter extrudates on a pyramidal cross-hatched plate (where $\theta = 28^o$). They also suggested that the differences may be due to the different pellet forming routes (see Figure 10 in Zhang *et al*., 2016b).

4.5 Discussion

The effects of the relative dimension of extrudates to the protuberances on spheronisation yield, pellet size and shape distributions, pellet surface tensile strength and surface morphology have been investigated. Plots of the yield, surface tensile strength, CQV of d_{CE} and CQV of *AR* against the geometrical factors are given in Figure 7.

The spheronisation yield varies with extrudate diameter when a given plate is used. The differences observed for flat plate indicate the influence of extrudate rheology and breakage on pellets. The effect of d^* and D^*on spheronisation yield is significant (as supported by ANOVA), and similar trends were observed with plates with similar θ (Figure 7). For plates A, B, E and F, all with $\theta \leq 28^o$, spheronisation yields decrease significantly as D/d^* and D/D^* increase, especially at $D/d^* > 1.2$ and $D/D^* > 1.6$ (Figure 7) when extrudates and pellets are less likely to stay in the furrows. For plates C and D, with $\theta \geq 45°$, the yields increase with D/d^* and D/D^*, and remain around 99% when both D/d^* and D/D^* are larger than 0.80.

A large amount of oversized pellets were obtained with the 2.5 mm extrudates using plates C

and D. These gave the highest yields, suggesting that collisions on these plates promoted less attrition. For plates other than C and D, the effect of D on median d_{CE}/D is significant. The reason why a small median d_{CE} is observed with D = 2.5 mm for plates X, A, B and E requires further investigation. Plate protuberance sizes and extrusion strain show little effect on aspect ratio.

For plates A, B and E, the CQV for d_{CE} varies with D/d^* and D/D^*, however, there is no consistent correlation (see Figure 7). As the protuberances are sharp, with $\theta \leq 28^o$, collisions between pellets and protuberances promote shape change, attrition and formation of fines, as well as breakage. Both spheronisation yield and pellet size distribution width are therefore reduced. There is common ground here with the literature on the erosion of surfaces by solid particle impact, *e.g.* Humphrey [31], where the particle is hard and the surface is relatively soft: in spheronisation the reverse applies.

Although the CQV of d_{CE} of plates C and D gradually decreases with increasing D/d^* and D/D^* (Figure 7), this is accompanied by oversized pellet generation. This suggests that collisions with the less sharp protuberances tend to promote rounding and attachment of fines. As a result, large pellets are produced and the yields are relatively constant for D/d^* and $D/D^* > 0.80$.

The pellets from flat plates show broader size and aspect ratio ranges, indicating the importance of the furrows in promoting breakage and collisions involved in rounding.

The extrudate diameter, which reflects the extrusion stain experienced by the material, shows a statistically significant effect on pellet tensile strength. Plates with more oblique protuberance angles, such as plates X and D, generated pellets with few surface defects. For plates with

$\theta \leq 45^{o}$, pellet surface morphology varies with D and d^{*}. Pellets with $D/d^{*}>1.5$ show smooth surfaces. This is possible due to the large amount of collisions between pellets in the rope. The results suggest that the sharpness of protuberances has an important role in the energy transition from plate to material. The protuberances with a similar θ show a similar correlation between pellet properties and the relative dimension of extrudates to protuberances. The current results do not indicate any correlation between the surface defects and surface tensile strength.

PCA was performed using dimensional groups (including S, W, H and D) and dimensionless ones (including $D/(S\text{-}W)$, D/H, D/d^{*}, D/D^{*} and θ). The results were inconclusive and more experimental data would be needed in order to identify principal components.

5. Conclusions

The effect of spheronisation plate geometry has been studied systematically for the first time using square patterned plates with different dimensions and extrudates of different diameters. The extrudate diameter (set by the screen hole size), plate protuberance dimensions and the ratio of the two all have noticeable effects on spheronisation behaviour and final pellet properties.

Pellet yield was found to be subject to two geometrical factors. Material can be lost through the gap between the rotating plate and the spheroniser wall, so was noticeably larger for 1 mm extrudates. Similarly, plate patterns which promoted attrition – principally those with sharp protuberances – gave lower yields for a given extrudate size. Sharp protuberances tended to give a more narrow size distribution, which is a favourable outcome, so there is a trade-off involved in selecting the plate geometry.

Most of the pellets generated had acceptable shape characteristics for tableting and capsuling, as measured by automated image analysis. Electron microscopy inspection, however, indicated that several groups of pellets featured defects that would render them unacceptable for controlled drug release applications. Surface defects were evident appearing when $D/d^* < 1.5$ and $\theta \leq 45^{\circ}$. This result, and several others, highlights the link between protuberance geometry and extrudate diameter: the dimensionless ratios used in this work provide a basis for scale-up when D is varied. Several results for 2.5 mm extrudates differed from those obtained for smaller diameters, suggesting a change in spheronisation mechanism for these larger extrudates.

Although the same paste formulation was used in the tests, the surface tensile strength of pellets obtained from 1.0 mm extrudates was significantly larger, indicating that the rheology of the paste material differed from that of the other cases. This result is consistent with previous studies in the literature and demonstrates some of the complexities involved in scale up of these systems.

Acknowledgements

The project was supported by the Chinese government State Education Ministry Scientific Research Foundation for Returned Overseas Chinese Scholars and the Fundamental Research Fund for the Central Universities (Grant Number xjj2015055). Funding from the British Council for DIW for a visit to China which supported discussions is gratefully acknowledged.

Nomenclature

Roman

d_{CE}	Circle equivalent diameter of pellet	m
$\bar{d}_{CE}$	Mean circle equivalent diameter of pellets from a batch	m
d_{dry}	Diameter of a dry sphere with a volume equal to an extrudate of length D	m
d_D	Diameter of a sphere with a volume equal to an extrudate of length D	m
d^*	Critical pellet diameter	m
D	Diameter of screen holes/diameter of extrudates	m
D*	Critical extrudate diameter	m
D[3,2]	Sauter mean diameter	m
F	Test statistic	-
F_c	Average crushing force	N
H	Height of protuberances on plate surface	m
l	Length of an extrudate segment	m
L	Thickness of screen	m
L_{AC}	Length of AC in Figure A2	m
L_{AO}	Length of AO in Figure A2	m
L_{AP}	Length of AC in Figure A1	m
m_{ex}	Mass of extrudates	kg
m_p	Mass of spheronisation product	kg
P	Statistical significance	-
Q_1	The first quartile (25% percentile)	-
Q_3	The third quartile(75% percentile)	-
R	Radius of spheronisation plate	m
S	Spacing between protuberances on plate surface	m
w_{ex}	Water content of extrudates	%
w_p	Water content of spheronisation product	%
W	Width of top of protuberances on plate surface	m
Y	Yield of a pellet sample on a dry basis	%
$\bar{Y}$	Average yield of pellet samples from three repeated tests	%

Greek

α	Protuberance top surface area fraction	-
β	Angle indicated in Figure A2	degrees
δ	Angle indicated in Figure A1	degrees
σ_t	Pellet surface tensile strength	N/m^2
θ	Protuberance corner angle	degrees
ω	Plate rotational speed	rpm

References

[1] S. Muley, T. Nandgude, S. Poddar, Extrusion–spheronization a promising pelletization technique: In-depth review, Asian Journal of Pharmaceutical Sciences, 11(2016)684–699.

[2] D. I. Wilson, S. L. Rough, Extrusion–spheronisation, in: A.D. Salman, M.J. Hounslow (Eds.), Granulation. Elsevier, Amsterdam, 2007, pp. 189-210.

[3] I. Ghebre-Sellassie, Pellets: A general overview, in: I. Ghebre-Sellassie (Ed.), Pharmaceutical Pelletization Technology, Marcel Dekker, New York and Basel, 1989.

[4] A. Desire, B. Paillard, J. Bougaret, M. Baron, G. Couarraze, Extruder scale-up assessment in the process of extrusion–spheronization: comparison of radial and axial systems by a design of experiments approach, Drug Development and Industrial Pharmacy, 39(2)(2013)176–185.

[5] P. Vonk, C. P. F. Guillaume, J. S. Ramaker, H. Vromans, N. W. F. Kossen, Growth mechanisms of high-shear pelletisation, International Journal of Pharmaceutics, 157 (1)(1997)93-102.

[6] M. Zhang, S. Mascia, S. L. Rough, R. Ward, C. Seiler, D. I. Wilson, A novel lab-scale screen extruder for studying extrusion-spheronisation, International Journal of Pharmaceutics, 455(1-2)(2013)285-297.

[7] K. E. Fielden, J. M. Newton, R. C. Rowe, The influence of lactose particle-size on spheronization of extrudate processed by a ram extruder, International Journal of Pharmaceutics, 81(2-3)(1992)205-224.

[8] K. E. Fielden, J. M. Newton, R. C. Rowe, A comparison of the extrusion and spheronisation behavior of wet powder masses processed by a ram extruder and a cylinder extruder, International Journal of Pharmaceutics, 81(2-3)(1992)225-233.

[9] S. L. Rough, J. Bridgwater, D. I. Wilson, Effects of liquid phase migration on extrusion of microcrystalline cellulose pastes, International Journal of Pharmaceutics, 204(1-2)(2000)117-126.

[10] L. Rahman, P. Rowe, A. Cheyne, D. I. Wilson, Ram extrusion of potato starch dough through multi-holed dies, Food and Bioproducts Processing, 80(C1)(2002)12-19.

[11] M. Zhang, S. L. Rough, R. Ward, C. Seiler, D. I. Wilson, A comparison of ram extrusion by single-holed and multi-holed dies for extrusion-spheronisation of microcrystalline-based pastes, International Journal of Pharmaceutics, 416(1)(2011)210-222.

[12] A. Engländer, A. Burbidge, S. Blackburn, A preliminary evaluation of single screw paste extrusion, Institution of Chemical Engineers, 78(A)(2000)790-794.

[13] X. Weert, C. J. Lawrence, M. J. Adams, B. J. Briscoe, Screw extrusion of food powders: prediction and performance, Chemical Engineering Science, 56(5)(2001)1933-1949.

[14] A. J. Botten, A. S., Burbidge, S. Blackburn, A model to predict the pressure development in single screw extrusion, Journal of Materials Processing Technology, 135(2-3)(2003)284-290.

[15] J. J. Benbow, J. Bridgwater, Paste Flow and Extrusion, Clarendon Press, Oxford, 1993.

[16] E. I. Corwin, Granular flow in a rapidly rotated system with fixed walls, Physical Review E, 77(2008)031308.

[17] M. Koester, R. E. García, M. Thommes, Spheronization process particle kinematics determined by discrete element simulations and particle image velocimetry measurements, International Journal of Pharmaceutics, 477(1-2)(2014)81-87.

[18] C.L.S. Lau, Q. Yu, V. Y. Lister, S. L. Rough, D. I. Wilson, M. Zhang, The evolution of pellet size and shape during spheronisation of an extruded microcrystalline cellulose paste, Chemical Engineering Research and Design, 92(2014)2413-2424.

[19] M. P. Bryan, L. N. Atherton, S. Duffield, S. L. Rough, D. I. Wilson, Stages in spheronisation: evolution of pellet size and shape during spheronisation of micro-crystalline cellulose-based paste extrudates, Powder Technology, 270(2015)163-175.

[20] J. Parkin, K. S. Widjaja, M. P. Bryan, S. L. Rough, D. I. Wilson, Experimental validation of a dimensional analysis of spheronisation of cylindrical extrudates, Powder Technology, 298(2016)73-83.

[21] H. Michie, F. Podczeck, J. M. Newton, The influence of plate design on the properties of pellets produced by extrusion and spheronization, International Journal of Pharmaceutics, 434(1–2)(2012)175-182.

[22] C. Schmidt, P. Kleinebudde, Comparison between a twin-screw extruder and a rotary ring die press. Part II: Influence of process variables, European Journal of Pharmaceutics and Biopharmaceutics, 45(2)(1998)173-179.

[23] C.V. Liew, S. M. Chua, P. W. S. Heng, Elucidation of spheroid formation with and without the extrusion step, AAPS PharmSciTech, 8(2007)1-10.

[24] M. Zhang, Y. Li, J. F. Xing, S. L. Rough, D. I. Wilson, Influence of plate surface protuberance size and shape on the production of pellets by extrusion-spheronisation, Chemical Engineering Research and Design, 109(2016)97-107.

[25] M. Zhang, D. I. Wilson, R. Ward, C. Seiler, S. L. Rough, A comparison of screen and ram extrusion-spheronisation of simple pharmaceutical pastes based on microcrystalline cellulose, International Journal of Pharmaceutics, 456(2)(2013)489-498.

[26] M. Zhang, Y. Li, Spheronisation of a basket screen-extruded paste using screens of different hole diameters, Powder Technology, 299(2016)199-209.

[27] D. G. Bonett, Confidence interval for a coefficient of quartile variation, Computational Statistics & Data Analysis, 50(11)(2006)2953-2957.

[28] M. Salako, F. Podczeck, J. M. Newton, Investigations into the deformability and tensile strength of pellets, International Journal of Pharmaceutics, 168(1998)49-57.

[29] M. P. Bryan, M. D. Kent, J. Rickenbach, G. Rimmer, D. I. Wilson, S. L. Rough, The effect of mixing on the extrusion-spheronisation of a micro-crystalline cellulose paste, International Journal of Pharmaceutics, 479(1)(2015)1-10.

[30] R. Chopra, F. Podczeck, J. M. Newton, G. Alderborn, The influence of pellet shape and film coating on the filling of pellets into hard shell capsules, European Journal of Pharmaceutics and Biopharmaceutics, 53(2002)327-333.

[31] J. Humphrey, Fundamentals of fluid motion in erosion by solid particle impact, International Journal of Heat and Fluid Flow, 11(3)(1990)170–195.

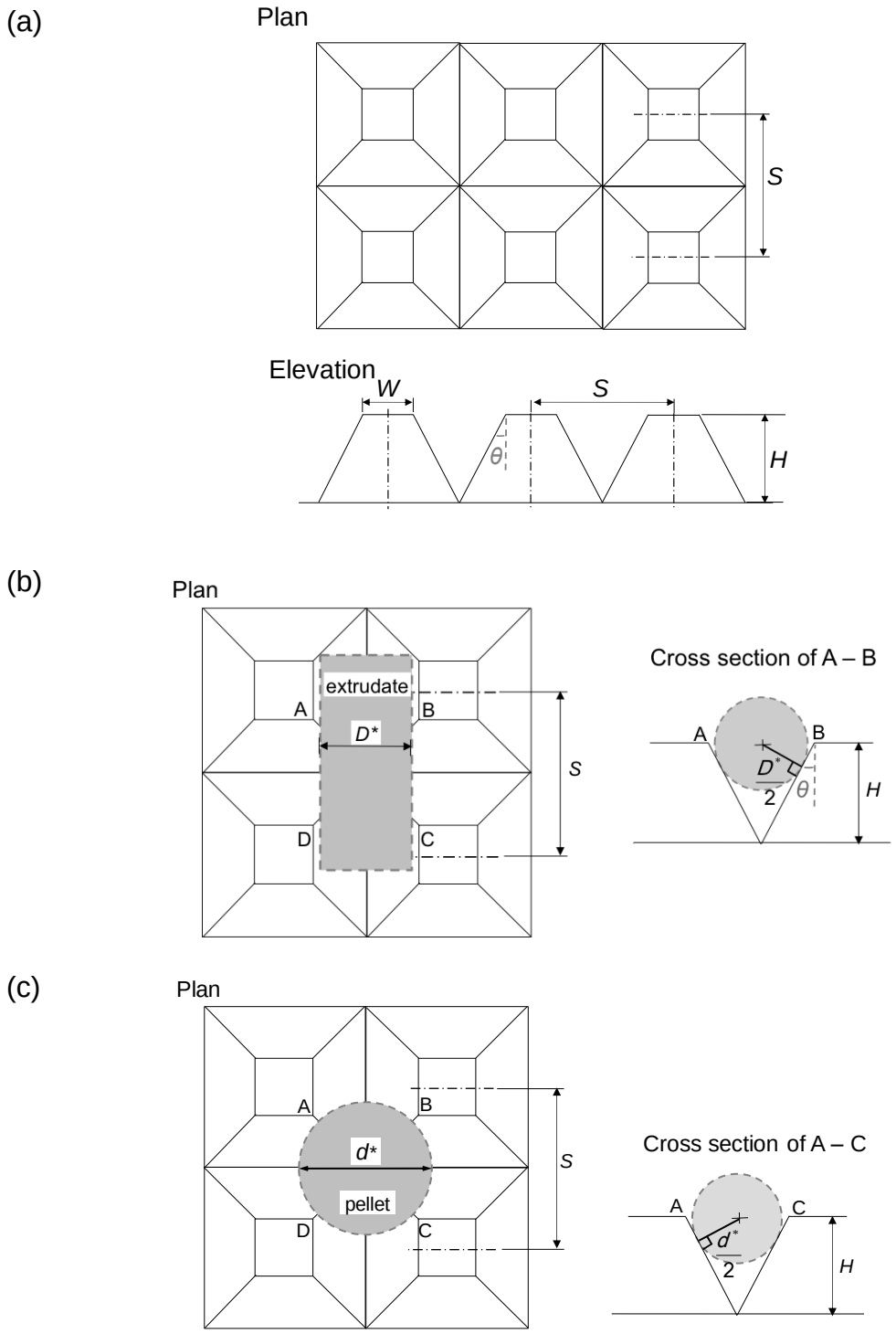

Figure 1 Schematics of protuberance pattern and dimensions (a) plan and elevation views; (b) schematic showing calculation of cylindrical extrudate with diameter D lodged in furrow; (c) schematic showing calculation of sphere of diameter d* lodged in 'seat'.*

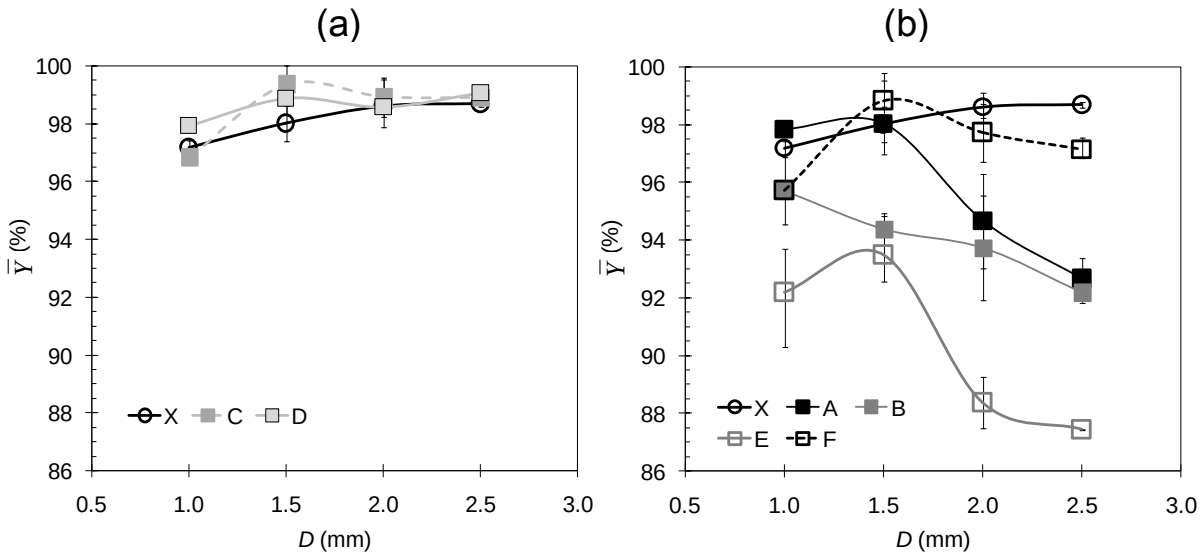

Figure 2 Spheronisation yield on a dry basis for (a) plates X, D (θ = 63^o, D = 1.8 mm) and C (θ = 45^o, D* = 1.4 mm), and (b) X, A (θ = 28^o, D* <1 mm), B (θ= 27^o, D* < 1. mm), E (θ = 14^o, D* < 1. mm), F (θ = 27^o, D* = 1.8 mm)*

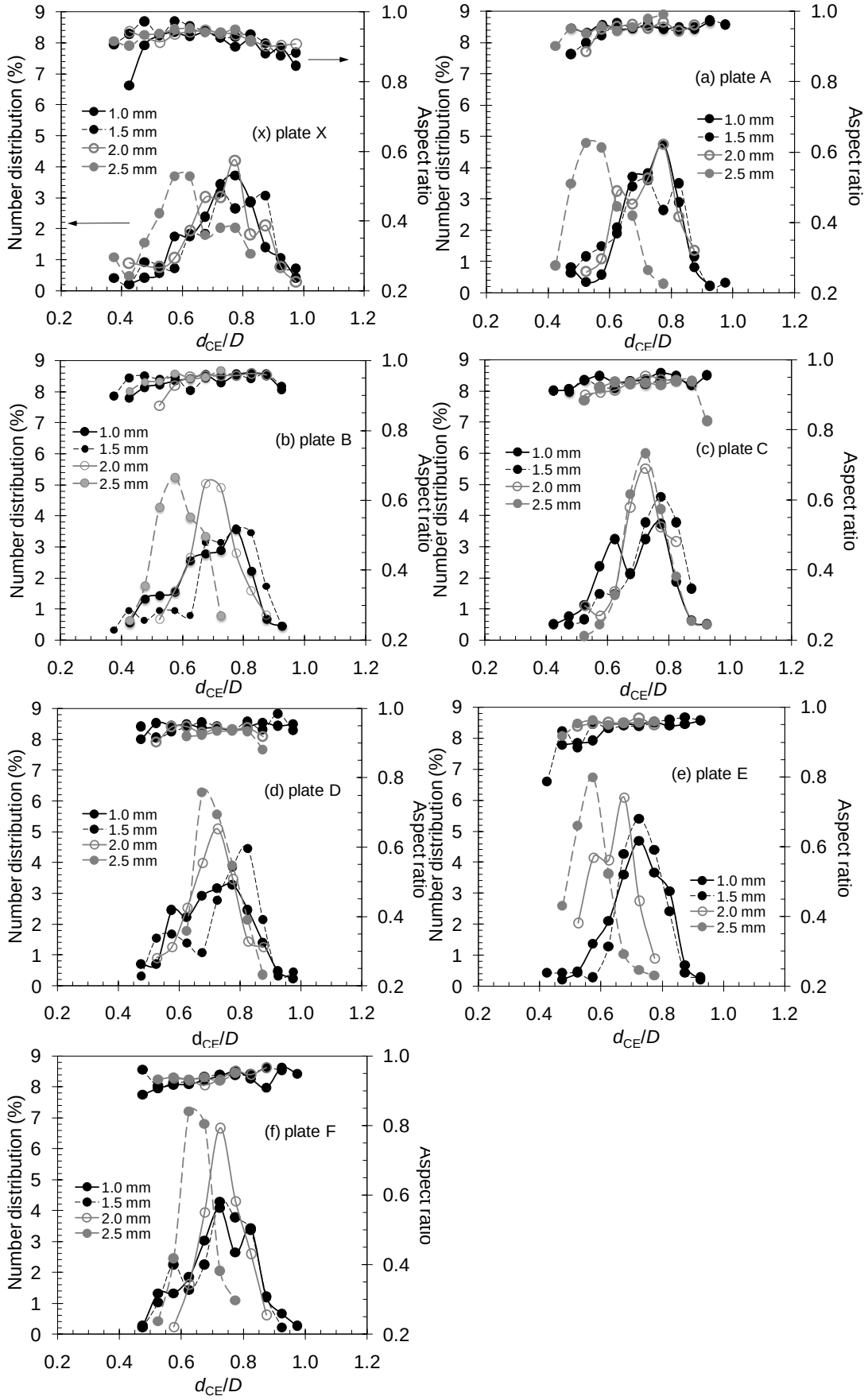

Figure 3 Size and shape distributions of pellets obtained from spheronisation using plate X (x), A(a), B(b), C(c), D(d), E(e) and F(f). Sizes are plotted in dimensionless form, d_{CE}/D.

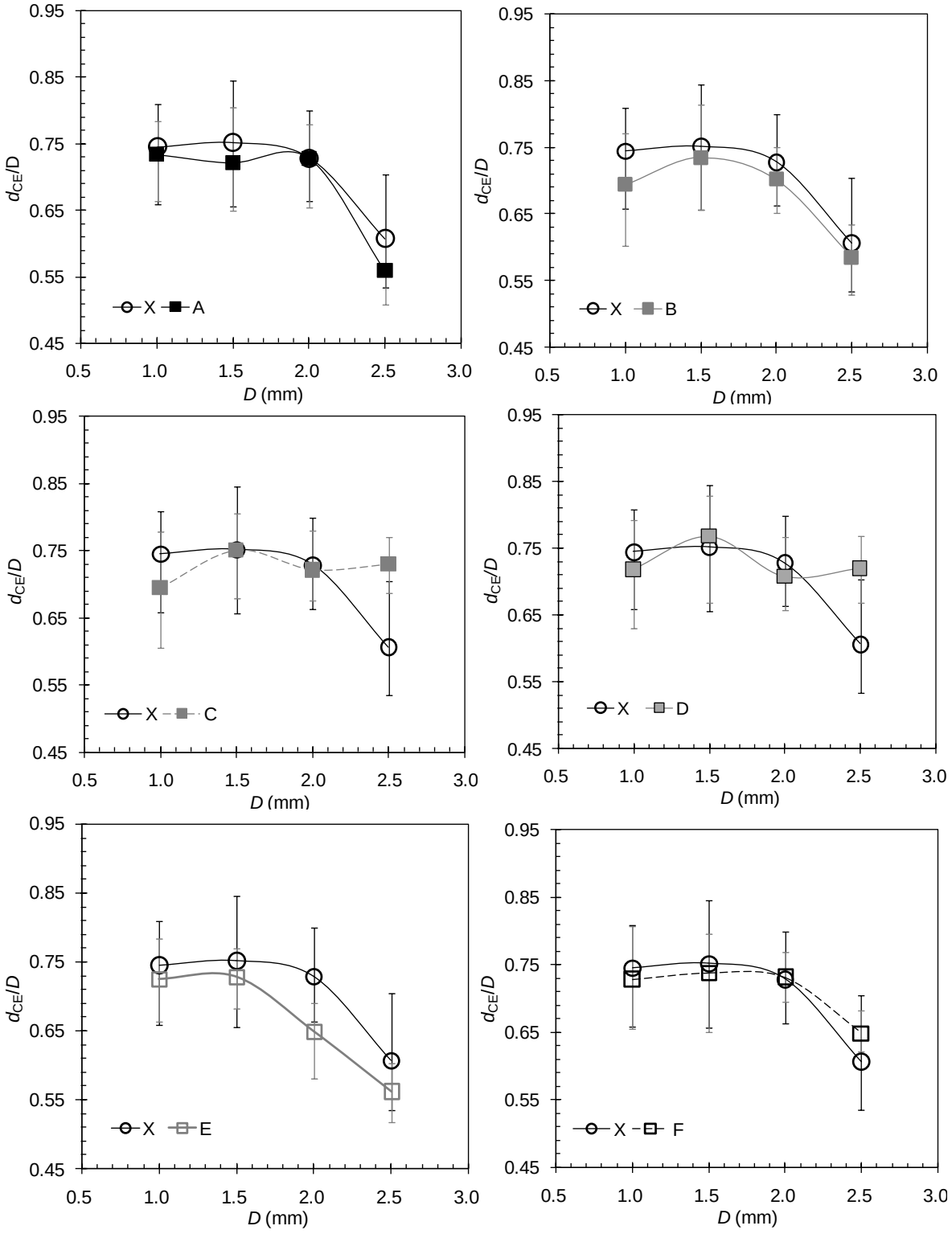

Figure 4 Plots of median d_{CE}/D against screen hole diameter. Pellets obtained from plates (a) A and X, (b) B and X, (c) C and X, (d) D and X, (e) E and X and (f) F and X. Error bars represent the 25% and 75% percentile values.

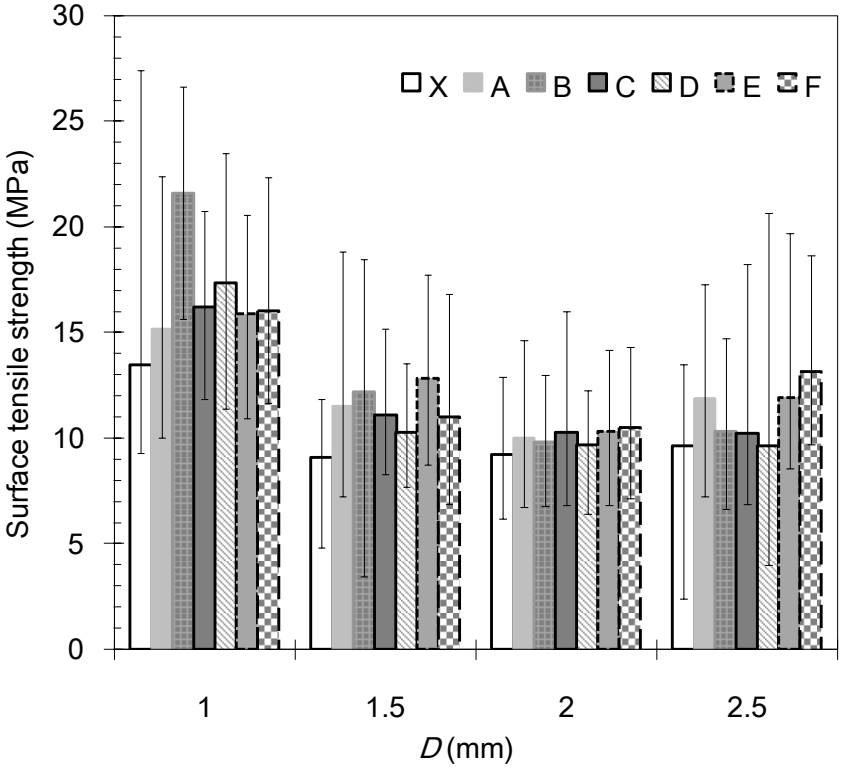

Figure 5 Surface tensile strength of pellets obtained from spheronisation of extrudates with different diameters. Error bars represent data range.

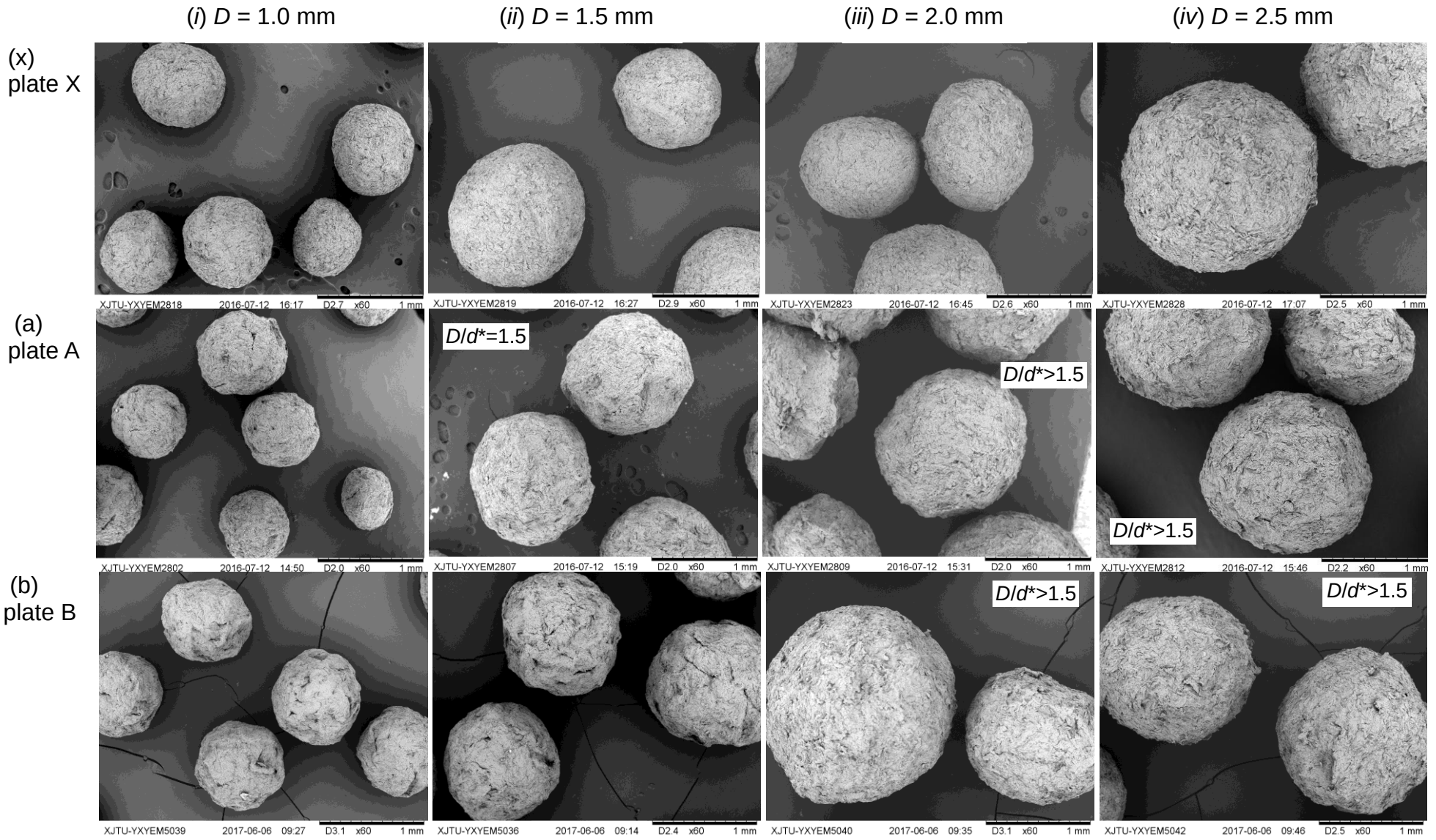

Figure 6 SEM images of dry pellets obtained from extrudates generated using screen hole diameters of (i) D = 1.0 mm, (ii) D = 1.5 mm,(iii) D = 2.0 mm (iv) D = 2.5 . Magnification 60×.

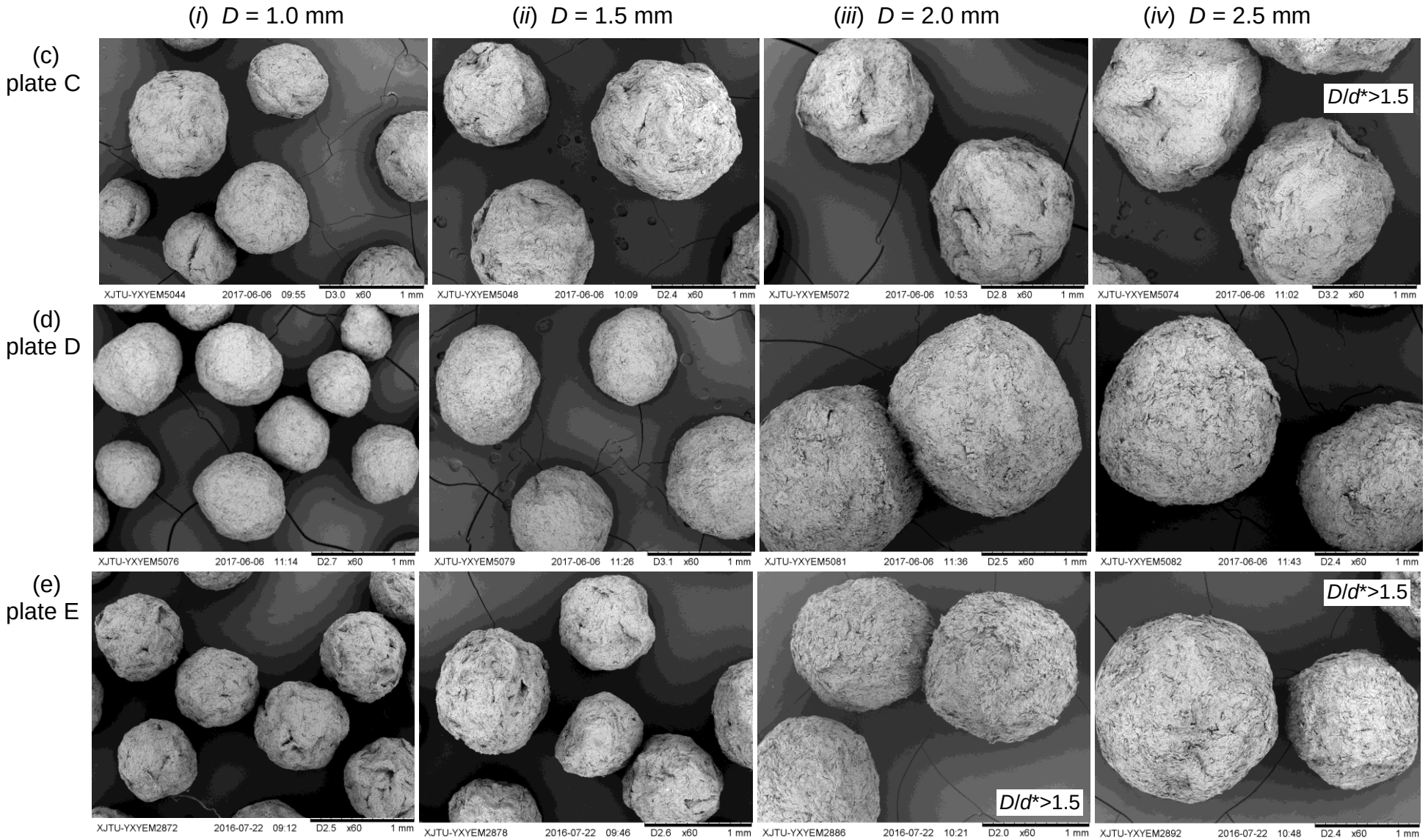

Figure 6 Continued.

(*i*) *D* = 1.0 mm (*ii*) *D* = 1.5 mm (*iii*) *D* = 2.0 mm (*iv*) *D* = 2.5 mm

(f) plate F

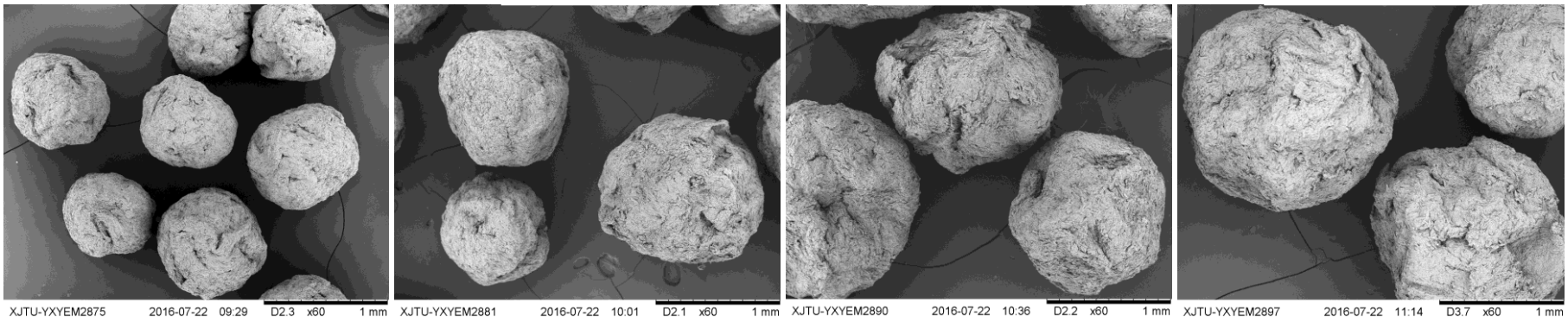

Figure 6 Continued.

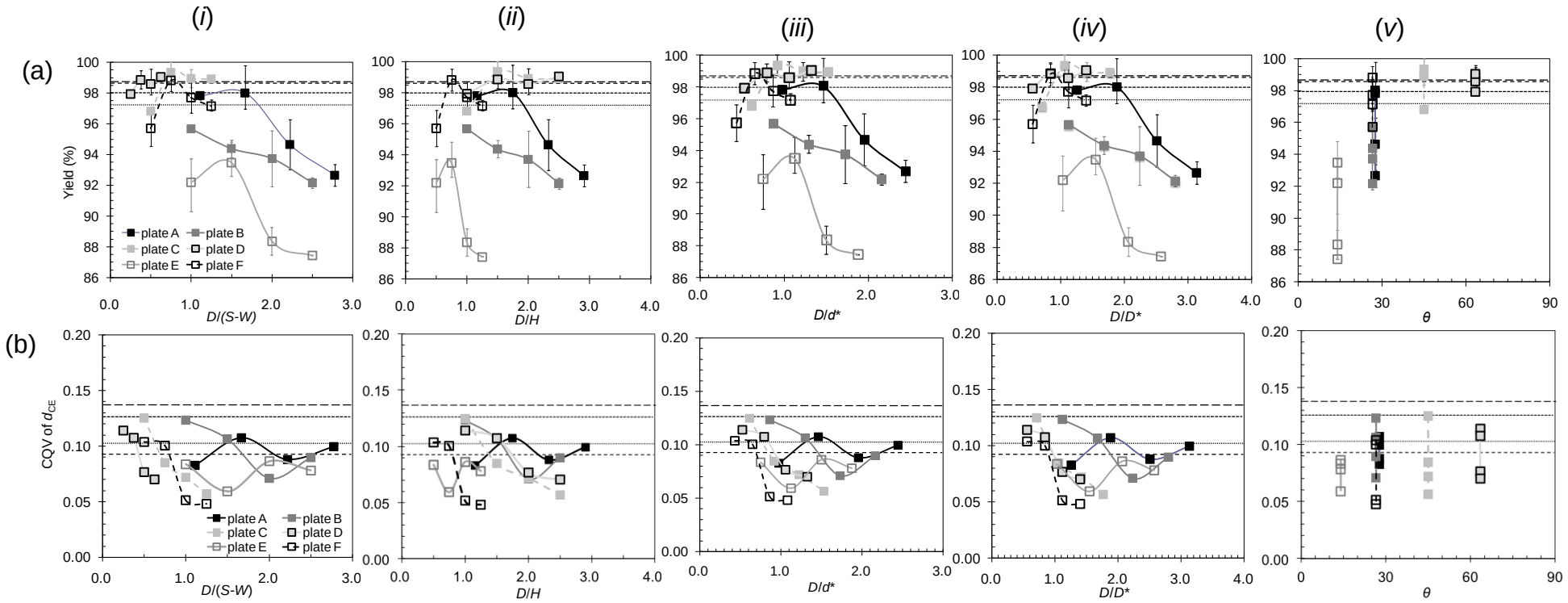

Figure 7 Plots of (a)yield, (b) CQV of d_{CE}, (c) CQV of AR and (d) surface tensile strength against dimensionless groups of (i) D/(S-W), (ii) D/H, (iii) D/D, (iv) D/d* and (v) θ. Dotted lines – data of plate X for D = 1.0 mm extrudates; short dashes – data of plate X for D = 1.5 mm extrudates; long dashes – data of plate X for D = 2.0 mm extrudates; and very long dashes – data of plate X for D = 2.5 mm extrudates.*

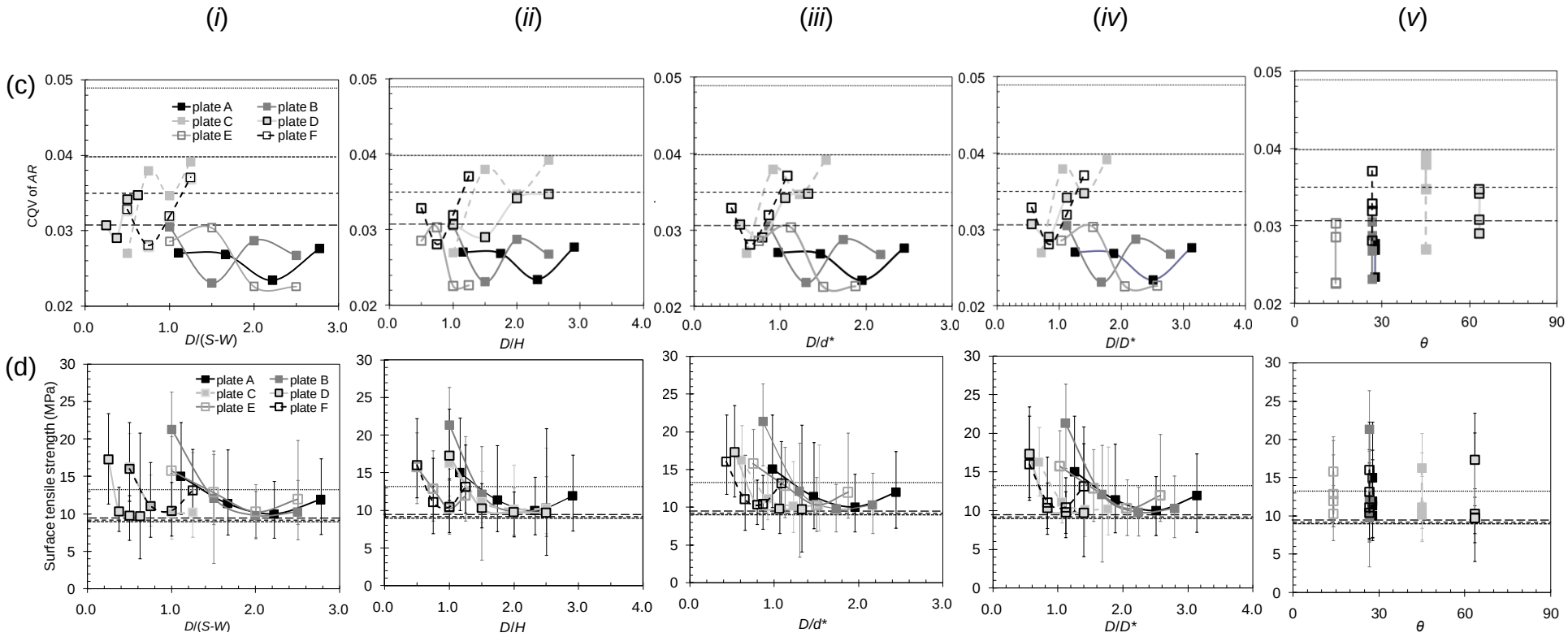

Figure 7 Continued.

Table 1 Investigations of influence of spheronisation plate geometry on pellet yield and properties (All dimensions are in mm unless otherwise stated). Microcrystalline cellulose (MCC) PH101 was used in all formulations.

Source	Paste formulation (w/w)	Extruder	Spheroniser plate diameter	Plate hatching pattern/pertuberance shape	Plate protuberance dimensions							Spheronisation condtions		Extrudate diameter, *D*	Pellet properties			
					W	*S*	*H*	*d**	*D**	α (-)	θ (-)	rim speed, *V* (m s^{-1})	time, *t* (min)		Yield (%)	Median pellet diameter	Aspect ratio* (-)	Surface tensile strength (MPa)
[1]Schmidt and Kleinebudde (1998)	lactose-Monohydrate:MCC: water=70:30:149	Twin-screw (ZE 25 × 18 D, Berstorff)	320 (Nica S320)	cross-hatched, pyramidal shape	1.9	3.5	0.8	1.3	1.1	0.29	45°	10.1	5	NG**	-	1.2	0.92	-
												13.4			-	1.4	0.91	-
			300 (Schlüter RM-300)		1.25	3.0	1.5	1.9	1.5	0.14	60°	10.1			-	1.7	0.88	-
												13.4			-	2.0	0.88	-
[2]Liew *et al*. (2007)	MCC:lactose monhydrate:water= 25:75:38	screen (GEA-Niro,E140)	320 (GEA-Niro,S320)	cross-hatched, pyramidal shape	1.0	3.0	0.5	0.94	0.89	0.11	63°	10.1	10	1	-	0.88	0.92	1.0
			275 (Aeromatic-Fielder, MP1)	Teardrop-drop (edges rounded)	base max. width = 8 ; base length = 14; *H* = 2.75 mm							11.4	20	1	-	0.77	0.90	0.9
[3]Michie *et al*. (2012)	diclofenac sodium:lactose monohydrate:MCC: water = 1:4:15:13.5	screen (Caleva, model 10)	225 (Caleva, model 250)	cross-hatched	NG							11.8	12	1.0	76	1.2	0.91	3.8
														1.5	58	1.3	0.92	4.6
				radial-hatched										1.0	84	1.2	0.93	3.8
														1.5	70	1.2	0.93	4.7
				striated edge										1.0	94	1.1	0.92	3.3
														1.5	37	1.5	0.90	4.7
[4]Zhang *et al*. (2016a)	MCC:water = 45:55	screen (Cheng Hang Xin Rong Hua, ZLB-80)	120 (Chong Qing Li Pu,R-120)	cross-hatched, pyramidal shape	0.5	1.4	0.86	1.0	0.79	0.13	27°	10.0	12	1.0	98	0.69	0.94	-
														2.0	96	0.70	0.95	-
				cross-hatched, small studs	0.5	1.4	0.86	1.3	0.90	0.13	0°			1.0	96	0.69	0.95	-
														2.0	93	0.68	0.93	-
				cross-hatched, larger studs	2.0	5.0	1.0	4.2	3.0	0.16	0°			1.0	99	0.76	0.86	-
														2.0	99	0.76	0.93	-
				cross-hatched, saw-toothed	0	3.0	1.5	2.1	1.9	0	63°			1.0	97	0.57	0.79	-
														2.0	96	0.68	0.94	-

1. More formulations were investigated by Schmidt and Kleinebudde [22]. Results for one which had a water content similar to the water content of the paste investigated in current study is reported here.
2. Pellet size distribution was measured by sieving, and median diameter was estimated based on mass distribution; pellet tensile strength was estimated using $\sigma_{\text{t-mass}} = 0.4 \frac{F_c}{\pi \left(\frac{\bar{d}_{\text{mass}}}{2} \right)^2}$, where $\bar{d}_{\text{mass}}$ is mass median diameter.
3. The yield was defined as the percentage of pellets in the size range between 0.7 and 1.4 mm; median size was estimated based on mass distribution; pellet surface tensile strength in MPa is reported.
4. Yield is defined as the percentage of dry material obtained after spheronisation; pellet diameter was measured by image analysis, and median size was estimated based on number distribution.

* Image analysis was used to measure pellet aspect ratios in all studies
**NG – not given.

Table 2 Dimensions and characteristic lengths of spheroniser plate protuberances (see Figure 1).

Plate	*W* (mm)	*S* (mm)	*H* (mm)	*S-W* (mm)	*d** (mm)	*D** (mm)	W^2 (mm^2)	θ (degrees)	α (-)
X	0	∞	0	∞	-	-	0	90	0
A	0.5	1.4	0.86	0.9	1.0	0.80	0.25	28	0.13
B	0.5	1.5	1.0	1.0	1.2	0.89	0.25	27	0.11
C	1.0	3.0	1.0	2.0	1.6	1.4	1.0	45	0.11
D	2.0	6.0	1.0	4.0	1.9	1.8	4.0	63	0.11
E	0.5	1.5	2.0	1.0	1.3	0.97	0.25	14	0.11
F	1.0	3.0	2.0	2.0	2.3	1.8	1.0	27	0.11

Table 3 Screen dimensions

Hole diameter , *D* (mm)	Thickness*, *L* (mm)	*L/D* (-)	Percentage of the area occupied by holes on the screen (%)
1.0	1.2	1.20	19.0%
1.5	1.2	0.80	24.2%
2.0	1.2	0.60	24.5%
2.5	1.2	0.48	55.4%

*Thickness variation ± 0.2 mm.

Table 4 Mass percentage of dry fines (<0.355) mm and large particles (>2.0 mm)

Plate	*D* = 1.0 mm		1.5 mm		2.0 mm		2.5 mm	
	fines (%)	large particles (%)	fines (%)	large particles (%)	fines (%)	large particles (%)	fines (%)	large particles (%)
X	0	0	0	0	0	0.1	4.3	0
A	0.2	0	0.1	0	0	0.3	0	2.0
B	0.3	0.1	0	0	0	0.3	0	0.1
C	0.2	0	0	0	0	0.4	0	31. 2
D	0.1	0	0.2	0	0.1	1.4	0	39.8
E	0	0	0	0	0	0	0	0.2
F	0. 2	0.2	0	0	0	0	0	4.8

Table 5 Summary of characterisics of the pellet size distributions curves given in Figure 3.

Plates	*D* (mm)			
	1.0	1.5	2.0	2.5
X	U+S	B+S	B+S	T
A	B+S	B	B	U+S
B	U+S	T+S	U	U+S
C	B	U+S	U	U
D	B	B	U	U
E	U+S	U	U+S	U
F	B+S	B+S	U	U

U: unimodal distribution; B: biomdal distribution; S: shoulder(s) on the distribution curve.

Table 6 Results of LSD test of pellet surface tensile strength

Batches compared			*P* for LSD test
D (mm)		*D* (mm)	
1.0	*vs*	1.5	5.29*
		2.0	6.46*
		2.5	5.45*
1.5	*vs*	1.0	-5.29*
		2.0	1.17
		2.5	0.16
2.0	*vs*	1.0	-6.46*
		1.5	1.17
		2.5	-1.01
2.5	*vs*	1.0	-5.45*
		1.5	-0.16
		2.0	1.01

* The mean difference is significant at the 0.05 level.

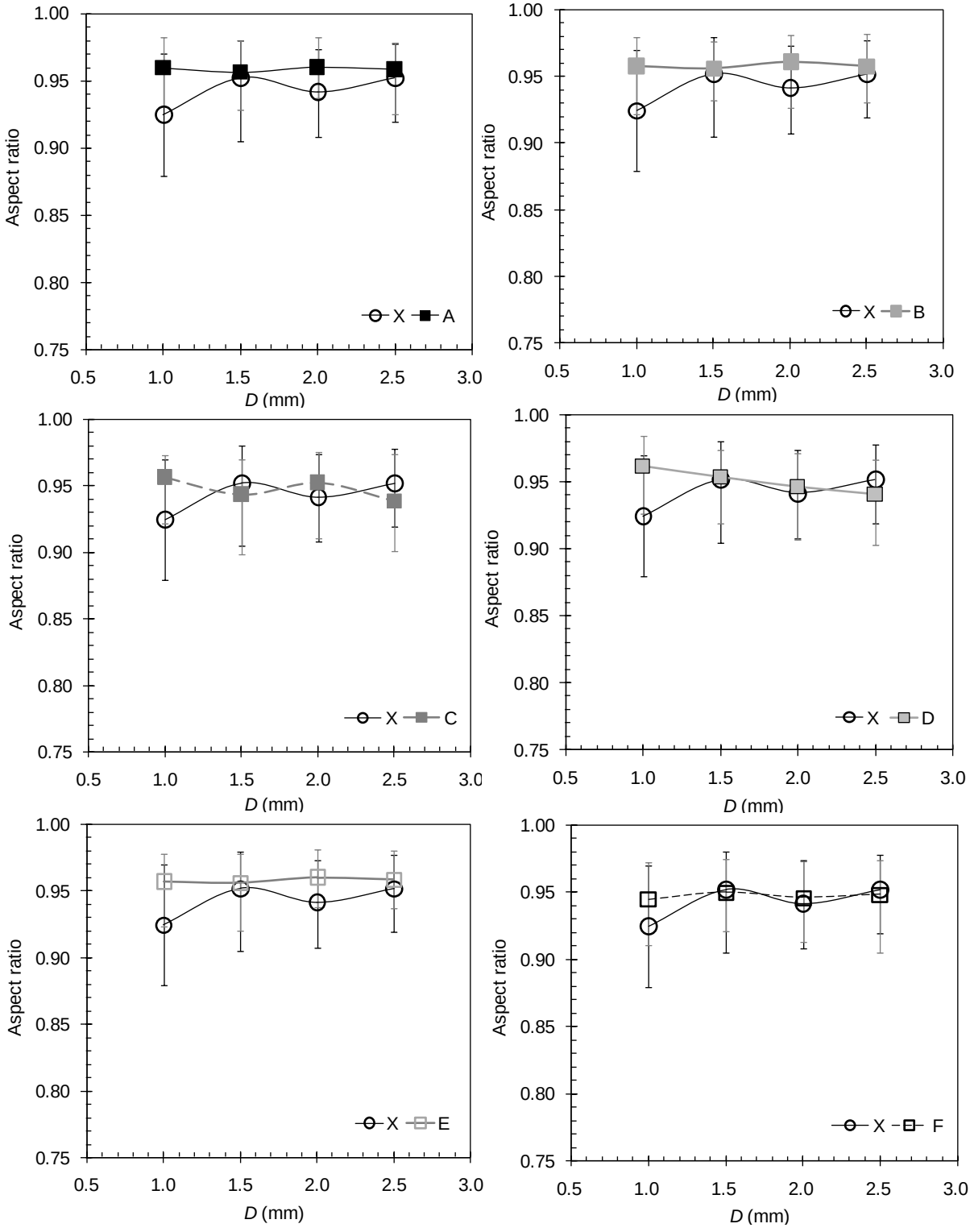

Supplementary Figure S1 Plots of median pellet aspect ratio against screen hole diameter. Data for X plotted in each as reference: (a) A, (b) B, (c) C, (d) D, (e) E,(f) F. Error bars represent the 25% and 75% percentile values. ANOVA analysis indicated that the effect of D on aspect ratio range is not significant (F = 0.307, P = 0.820).

Appendix:

Equation 3:

$$\cos\delta = \frac{D^*/2}{(S-W)/2} = \frac{D^*}{(S-W)}$$

$$L_{AP} = \sqrt{\left(\frac{S-W}{2}\right)^2 + H^2}$$

where L_{AP} is the length of AP in Figure A1.

also

$$\cos\delta = \frac{H}{\sqrt{\left(\frac{S-W}{2}\right)^2 + H^2}}$$

so

$$D^* = \frac{H(S-W)}{\sqrt{\left(\frac{S-W}{2}\right)^2 + H^2}}$$

$$= \left[\frac{1}{4H^2} + \frac{1}{(S-W)^2}\right]^{-1/2}$$

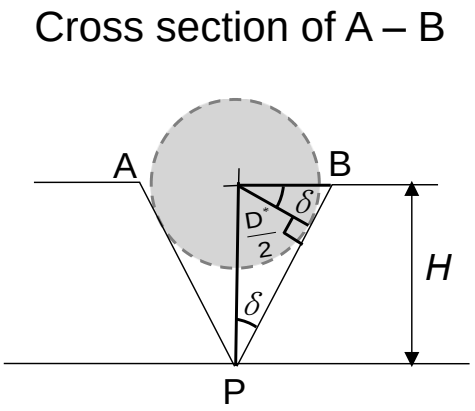

Figure A1 Schematics for calculation of D^*.

Equation 4:

$$L_{AC} = \sqrt{2}\left(S\text{-}W\right)$$

where L_{AC} is the length of AC in Figure A2.

$$L_{AO} = \sqrt{\left(\frac{\sqrt{2}\left(S\text{-}W\right)}{2}\right)^2 + H^2}$$
$$= \sqrt{\frac{\left(S\text{-}W\right)^2}{2} + H^2}$$

where L_{AO} is the length of AO in Figure A2.

$$\cos\beta = \frac{d^*/2}{L_{AC}/2} = \frac{d^*}{L_{AC}} = \frac{d^*}{\sqrt{2}\left(S\text{-}W\right)}$$

also

$$\cos\beta = \frac{H}{\sqrt{\frac{\left(S\text{-}W\right)^2}{2} + H^2}}$$

so

$$d^* = \frac{\sqrt{2}\left(S\text{-}W\right)H}{\sqrt{\frac{\left(S\text{-}W\right)^2}{2} + H^2}}$$
$$= \left[\frac{1}{4H^2} + \frac{1}{2(S\text{-}W)^2}\right]^{-1/2}$$

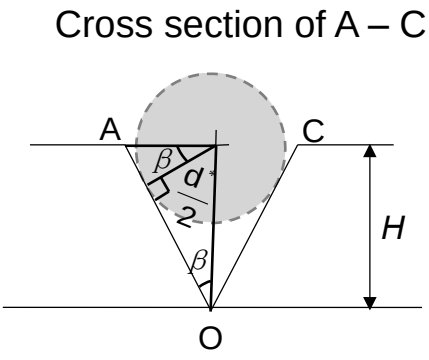

Figure A2 Schematics for calculation of d^*.